RSC Advances

PAPER

View Article Online
View Journal | View Issue

Cite this: *RSC Adv.*, 2022, **12**, 32230

Spectral filtering method for improvement of detection accuracy of Mg, Cu, Mn and Cr elements in aluminum alloys using femtosecond LIBS

Jieqi Yao, [a] Qi Yang, [ab] Xiaoyong He, *[a] Jiale Li, [a] Dongxiong Ling,[a] Dongshan Wei [a] and Yipeng Liao[c]

In this work, magnesium (Mg), copper (Cu), manganese (Mn) and chromium (Cr) in aluminum alloy samples were quantified by femtosecond laser-induced breakdown spectroscopy (fs-LIBS). The different parameters affecting the experimental results, including the laser pulse energy, moving speed of the 2D platform and spectral average number were optimized. The background signal preprocessing methods of median filtering (MF corrected) and Savitzky–Golay filtering (SG corrected) algorithms were used and the effect of the LIBS spectral analysis in the experiment investigated. The calibration curves of Mg, Cu, Mn and Cr elements were established separately and their corresponding detection limits (LODs) were calculated. After background correction, the LODs of Mg, Cu, Mn and Cr elements in MF corrected were 54.52, 11.69, 7.33 and 27.72 ppm, and in SG corrected were 59.15, 17.48, 14.75 and 31.97 ppm. The LODs of these elements in MF corrected and SG corrected have 1.4–5.2 and 1.2–2.5 improvement factors compared to those obtained using the fs-LIBS technique. This work demonstrates that background signal preprocessing methods are very helpful for improving analytical sensitivity and accuracy in quantitative analyses of aluminum alloys.

Received 14th September 2022
Accepted 1st November 2022

DOI: 10.1039/d2ra05792a

rsc.li/rsc-advances

1. Introduction

Laser-induced breakdown spectroscopy (LIBS) is also known as laser-induced plasma spectroscopy and laser spark spectroscopy. It is a highly accurate elemental analysis technique based on atomic emission spectroscopy. Its advantage of enabling microdestructive testing and multi-element analysis have made it popular in recent decades. The elemental analysis technology of LIBS has been widely used for applications in food safety,[1,2] industrial testing,[3–5] geological correlation analysis,[6,7] environmental quality monitoring,[8–10] cultural heritage,[11,12] materials science,[13] biomedicine[14] and many other fields. Related basic research in LIBS has been continuously advancing.

Femtosecond lasers have some important characteristics such as low thermal effect, high peak power and stability. LIBS using a femtosecond laser source is usually termed fs-LIBS. Fs-LIBS produces very little damage to samples with, absence of fractional evaporation, even can realize micron- and nanometer-scale precision detection. In light of the many advantages of the femtosecond laser and fs-LIBS described above, they are widely used by researchers. Carvalho *et al.*[15] compared surface elemental mapping analysis of spinach leaves after the action of ns-LIBS and fs-LIBS and found that established higher accuracy and less uncertainty on mass fractions quantification from fs-LIBS, regardless of using the classical least squares regression model or multivariate partial least squares (PLS) regression models. Scaffidi *et al.*[16] observed minor reductions in atomic emission and as much as 15 fold improvements in mass removal for fs single-pulse LIBS of heated brass and aluminum samples. Finney *et al.*[17] statistically analyzed the uranium detection efficiency based on several characteristic features in the plasma emission spectrum. They found that nearly 100% detection probability can be reached with 1% false-alarm probability in $\lesssim$1 second when using an 80 Hz laser and data acquisition system. Shaik *et al.*[18] used LIBS for the long- and close-range detection of explosive molecules (nitroimidazoles and nitropyrazoles). Different aspects influencing the LIBS signal strength at far distances such as fluence at target, the efficiency of collection system *etc.* are discussed. This demonstrates that any improvement to the LIBS signal will benefit the application.

Despite the many advantages of fs-LIBS, it is subject to multiple sources of interference during experiments. Most LIBS systems are exposed to air and subjected to ambient noise (water cooling, *etc.*) and atmospheric pressure during measurements. Current noise in the internal components of the instrument, noise in the photoelectric conversion process and

[a]*School of Electrical Engineering and Intelligentization, Dongguan University of Technology, Dongguan, 523808, China. E-mail: hxy@dgut.edu.cn*
[b]*Guangdong Provincial Key Laboratory of Nanophotonic Functional Materials and Devices, South China Normal University, Guangzhou, 510631, China*
[c]*School of Microelectronics, Shenzhen Institute of Information Technology, Shenzhen, 518172, China*

dark currents in the detector can all interfere with the accuracy of elemental analyses. Therefore, to obtain reliable results, it is essential to use preprocessing methods to reduce the noise in spectral data. Sun *et al.*[19] achieved the automatic deduction of a continuous background by removing the minimum points in the spectral line that are larger than the set threshold and accurately estimated varying continuum backgrounds over a wide range of wavelengths. Body *et al.*[20] showed that normalization of the overall plasma intensity could be effective, *i.e.*, normalization of the spectral intensity could reduce the interference of abnormal data. Schlenke et al.[21] utilized adaptive variable threshold denoising for spectral data using signal smoothing degree and mean square error analysis, with good denoising results. Yang *et al.*[22] studied LIBS spectra of lead-contaminated cabbage in the wavelength range of 400.45–410.98 nm, pre-treated by Savitzky–Golay (SG), which was experimentally shown to have good smoothing effects. To date, wavelet analysis techniques have been widely studied in spectral denoising processing, and good application results have also been achieved.[23–26]

In this study, the effect of the median filtering (MF corrected) and Savitzky–Golay (SG corrected) filtering algorithms on the denoising effect of the LIBS spectrum were compared. A femtosecond laser was used as the sample ablation source, and some standard aluminum alloy samples were used as the test samples. The effect of different experimental parameters on signal intensity were investigated in the experiment. After optimizing the experimental conditions, quantitative analysis of Mg, Cu, Mn and Cr in aluminum alloys was conducted, and two signal processing methods were analyzed. Compared with the original data, calibration curves were prepared, and their corresponding detection limits were calculated. The analytical performance of the two noise processing methods is evaluated and discussed in this paper.

2 The experimental setup diagram and background treatment methods

2.1 The experimental setup

The experimental setup of fs-LIBS is shown in Fig. 1. An ultrafast Ti: sapphire femtosecond laser (model Astrella) is used for the studies, with the pulse width of approximately 35 fs, laser center wavelength of 800 nm, and an output laser beam diameter of 10 mm. The repeated frequency was 1 kHz, and the maximum pulse energy output was 7.5 mJ. For the sample we used the aluminium alloy discs of 40 mm diameter and 3 mm thickness. We used a programmable X–Y mobile platform and fixed the aluminum alloy sample to be tested on it.

The coated mirrors were used to guide the femtosecond laser beam and focused on the sample surface through a quartz lens L1 ($f = 50$ mm). Transmitting a specific wavelength beam to L2 using a dichroic mirror. The plasma spectrum was collimated by shaping the beam into parallel light through a quartz lens L2 ($f = 150$ mm) and converging the beam through a quartz lens L3 ($f = 100$ mm). The converged plasma spectrum was then collected using an optical probe. Here, plasma spectra were recorded and processed by using a small portable three-channel fiber spectrometer (Avantes, Netherland, model 12012156U3, 1202157U3 and 1202158U3). Finally, the spectral data were analysed by a computer. The optimum experimental conditions were selected for the different experimental variables, the relative intensities of the different elements of the samples were analysed and their relative standard deviations were calculated. In turn, comparing with the original data, calibration curves were prepared, and their corresponding detection limits were calculated.

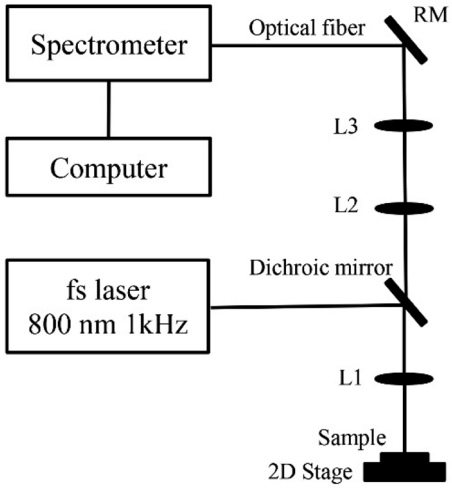

Fig. 1 Experimental setup diagram of fs-LIBS.

Six verified standard aluminum alloy samples were GBW(E) 020095, 020097, 020100, 020093, 020094, and 020101, purchased from Jinan Zhongbiao Technology Co., Ltd. The concentrations of Mg, Cu, Cr, and Mn elements in these standard samples are listed in Table 1. These samples were used to investigate parameter optimization, calibration curves preparation, detection limit calculations and evaluation of technical analysis.

2.2 Background processing methods

The spectral data obtained contains more random noise signals due to multiple interferences, which reduces the quality of the data. But then we need to get the type and content of the target element based on the qualitative and quantitative analysis of the signal. Therefore, the spectral information needs to be

Table 1 Concentrations of Mg, Cu, Cr, and Mn elements in six standard aluminum alloy samples (wt%)

Samples	Mg	Cu	Cr	Mn
GBW020093	0.544	2.850	0.000	0.292
GBW020094	0.341	2.080	0.001	0.521
GBW020095	5.910	0.019	0.050	0.642
GBW020097	4.180	0.057	0.260	0.471
GBW020100	2.210	0.144	0.214	0.292
GBW020101	1.620	0.174	0.117	0.216

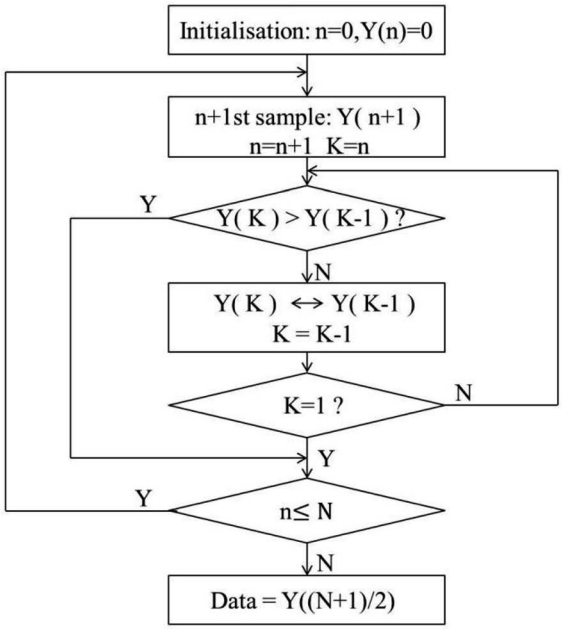

Fig. 2 Schematic flow diagram of the median filtering algorithm.

smoothed to reduce noise and improve the accuracy of the analysis. In this experiment, two methods of background noise signal processing were proposed.

2.2.1 Median filter algorithm (MF corrected). Fig. 2 shows the data processing steps of median filtering algorithm (MF). The MF is a nonlinear signal processing technology based on the statistical theory of ranking, which can effectively suppress noise; it is the optimal filter under the "minimum absolute error" criterion for optimal filtering. The basic principle is to replace the value of a point in a digital sequence with the median value of each point value in a neighborhood window of the point, thereby eliminating isolated noise points. The MF can filter spikes. The spectrally filtered data retain the changing trend of the original data but remove some of the effects of the spikes on the analysis at the same time.

2.2.2 Savitzky–Golay filter algorithm (SG corrected). The SG filtering algorithm is also a common method of noise signal processing. In this experiment, the SG algorithm was used to denoise the spectral data obtained by fs-LIBS technique. The SG filter was originally proposed by Savitzky and Golay in 1964. Since then, this algorithm has been widely used for data stream smoothing and denoising. It is a filtering method based on local polynomial least squares fitting in the time domain. Selecting the appropriate data span and degree of fitting can improve the processing effect of the SG filtering algorithm.[27]

The Savitzky–Golay algorithm can be derived as follows. Consider a set of 2 M + 1 data centered on $n = 0$, fit it with the following polynomial:

$$p(n) = \sum_{k=0}^{N} a_k \cdot n^k \quad (1)$$

The residuals of its least significant fit are:

$$\varepsilon_N = \sum_{n=-M}^{M} (p(n) - x[n])^2 = \sum_{n=-M}^{M} \left(\sum_{k=0}^{N} a_k \cdot n^k - x[n] \right)^2 \quad (2)$$

Convolution is used to obtain the constant term of the fitted polynomial, *i.e.*, a weighted average of the input data as follows:

$$y[n] = \sum_{m=-M}^{M} h[m] \cdot x[n-m] = \sum_{m=n-M}^{n+M} h[n-m] \cdot x[m] \quad (3)$$

The partial differentiator of the above equation, when simplified, is as follows:

$$\sum_{k=0}^{N} \left(\sum_{n=-M}^{M} n^{i+k} \right) \cdot a_k = \sum_{n=-M}^{M} n^i \cdot x[n] \quad (4)$$

where $i = 0, 1 \ldots N$.

Let $A = \{a_{ni}\}$, $a_{ni} = n^i$, $M \le n \le M$, $0 \le i \le N$, $B = A^T \cdot A$, then

$$b_{ki} = \sum_{n-M}^{M} a_{in} a_{nk} = \sum_{n-M}^{M} n^{i+k} = b_{ki} \quad (5)$$

Thus,

$$Ba = A^T \cdot Aa = A^T x \quad (6)$$

The estimated value of a is obtained by fitting with least-squares.

$$\hat{a} = \left(A^T A \right)^{-1} \cdot A^T x = Hx \quad (7)$$

where $\hat{a}$ is the estimate of a, and the estimate of x can be derived from eqn (6). Thus, one obtains that H is the coefficient of convolution.

3. Results and discussion

Experimental parameters, such as the speed of the 2D platform, the pulse of the fs laser and the spectra average number acquisitions, play a crucial role in the evaluation of the analytical performance of the technique. Therefore, in the fs-LIBS experiment, we analyzed the speed of the 2D stage, the pulse of the fs laser and the spectra average number acquisitions using a rigorously controlled variables approach and obtained optimized experimental parameters. Four atomic net signal spectral lines, including Mg I (285.21 nm), Cu I (324.75 nm), Mn I (403.44 nm) and Cr I (428.97 nm), were selected to test the experimental results under different parametric conditions, and the optimum experimental parameters were determined.

3.1 Influence of platform speed on spectral signal intensity

As the repetition rate of femtosecond laser is 1 kHz, and the overlapping focus of the laser pulse on the aluminum alloy sample affects the signal intensity, the aluminum alloy sample detection signal has a great relationship with the sample speed. To prevent signal weakening caused by overlapping focus positions and improve detection sensitivity, we set up a series

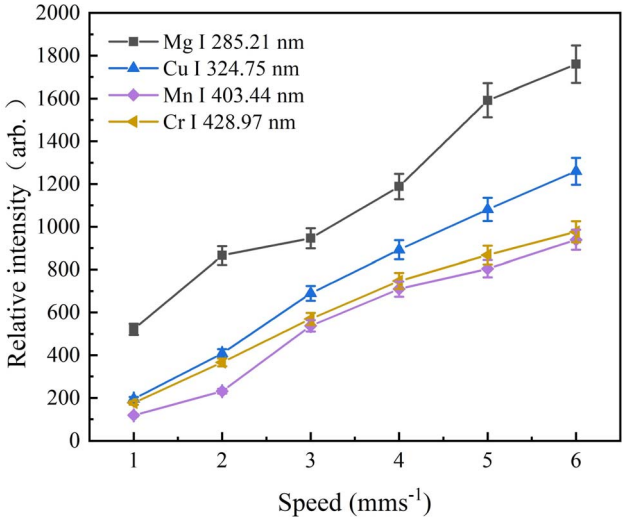

Fig. 3 Plots of signal intensities of Mg, Cu, Mn and Cr elements *versus* 2D mobile platform speed. Error bar shows the signal deviation of the multiple repeated measurements.

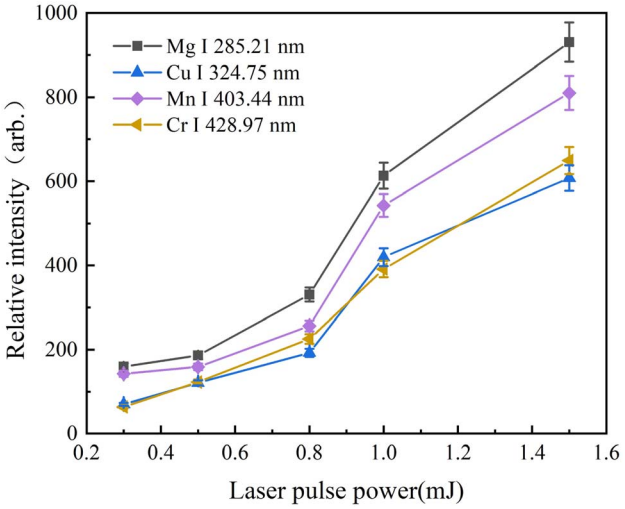

Fig. 4 Plots of signal intensities of Mg, Cu, Mn and Cr elements *versus* pulse energy of the femtosecond.

of experiments to investigate the effect of the speed of the sample on the 2D platform on the signal intensity. In the experiments, we kept the LIBS laser single pulse energy at 1.5 mJ and the integration time at 5 ms. The spectra were obtained by averaging over 500 repeated measurements and adjusting the moving speed of the stepper motor driving the 2D motion stage to 1–6 mm s^{-1}. Fig. 3 below shows the experimental results of the signal intensity at Mg I 285.21 nm, Cu I 324.75 nm, Mn I 403.44 nm, and Cr I 428.97 nm and the moving speed of the aluminum alloy sample. Fig. 3 shows that as the sample movement speed increased, the relative intensities of the four elements also increased. The diameter of the ablated crater on the sample surface was observed by the LIBS laser pulse through an optical microscope, which can explain the relationship between the reaction of four elements and the sample moving speed reflected in Fig. 3 above. When the moving speed of the sample is small, the positions of the pits ablated by two adjacent LIBS pulses overlap each other, and the previous pits will affect the LIBS laser pulse to break down and strip the sample to form plasma, thereby affecting the relative intensities of the four elements. When the sample travel speed is increased to 5 mm s^{-1}, the positions of the pits ablated by the two adjacent LIBS laser pulses no longer overlap. The location of the sample ablated with each LIBS laser pulse was new, resulting in the formation of the highest-intensity signal. At this time, the increase in the speed of the sample does not have a substantial effect, so the plasma signal tends to be stable.[28]

When it exceeded 6 mm s^{-1}, the motor of the 2D mobile platform became hot and instability. To protect the stability of the atomic signal intensity and durability of the 2D mobile platform, the speed was selected as 5 mm s^{-1} in the following experiments.

3.2 Influence of laser pulse energy on spectral signal intensity

If the selected laser pulse energy is too small, then the laser pulse energy density at the focus point cannot reach the breakdown threshold of the element to be measured. Even if a very sensitive detector is used or the frequency of the laser pulse is increased, the atom cannot be excited, resulting in a weak signal intensity, which makes it impossible to analyze the spectral information of the element. When the selected laser pulse energy is too large, although the intensity of the plasma emission signal is enhanced, it easily leads to saturation of some atomic or ion spectral lines due to the strong self-absorption effect, thereby reducing the sensitivity of the elemental analysis. Therefore, the selection of the appropriate laser single pulse energy is of great importance for improving the sensitivity of elemental analysis.

In this experiment, four atomic lines for Mg I (285.21 nm), Cu I (324.75 nm), Mn I (403.44 nm), and Cr I (428.97 nm) were studied with laser pulse energy of 0.3, 0.5, 0.8, 1.0 and 1.5 mJ. The speed of the 2D platform was fixed at 5 mm s^{-1}, the CCD integration time of the Avantes multichannel fiber optic spectrometer was 5 ms, and the spectrum was obtained by averaging 500 repeated measurements. The experimental results are shown in Fig. 4, where we find that the signal intensities of several elements increase with increasing laser single pulse energy. The signal strength here adopts the peak strength of the spectral line.

3.3 The advantage of the average number of spectra on the detection limit

The most common method to improve the measurement precision is to use the average of multiple spectral data in fiber spectrometer measurements, but this approach also increases the measurement time and is not conducive for industrial applications. To analyze the influence of the average number of

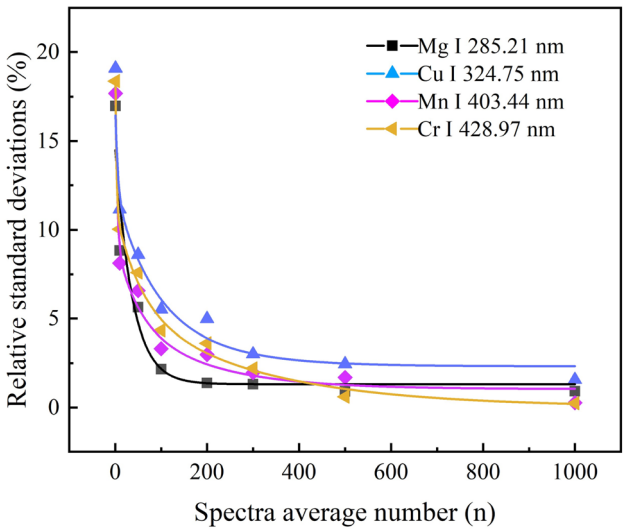

Fig. 5 Plots of signal intensities of Mg, Cu, Mn and Cr elements *versus* number of spectral averages.

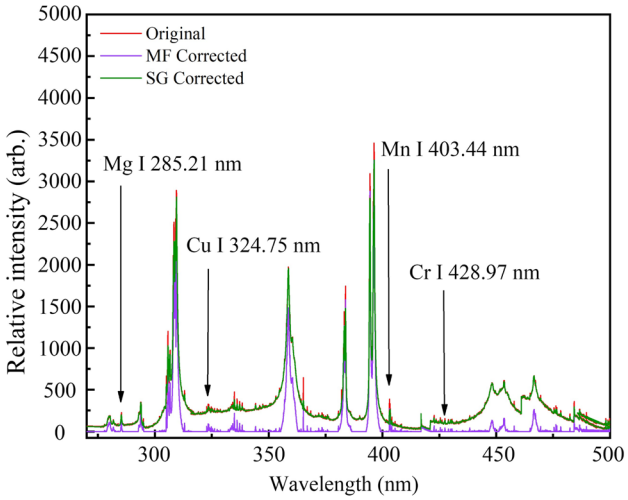

Fig. 6 The characteristic spectra of Mg, Cu, Mn and Cr elements in the aluminum alloy sample in the fs-LIBS system.

spectra on the precision of the fs-LIBS measurements, four atomic lines, Mg I (285.21 nm), Cu I (324.75 nm), Mn I (403.44 nm) and Cr I (428.97 nm), were still chosen for the study. At a laser single pulse energy of 1.5 mJ and an integration time of 5 ms, the average number of spectra were 1, 10, 50, 100, 200, 300, 500 and 1000, followed by 10 repeated measurements, and the precision was evaluated by the relative standard deviation values of these 10 repeated measurements. Fig. 5 shows the variation curve of the relative standard deviation of the spectral line intensities with increasing spectral averaging number. The standard deviations were high at the initial stage when the number of averages increased and fell rapidly as the number of spectra averaged increased, after which the behavior worsened. When the average number of spectra was 500, the relative standard deviation was clearly reduced, which indicated that the effect of increasing the average number of times to improve the measurement precision was not very obvious. The graphs below also show that the relative standard deviation values for the different spectral lines follow essentially the same pattern of variation with the number of spectral averages.

From the present experiment, it can be concluded that the multiple averaging methods of the spectral signal can effectively improve the precision of the measurement. According to the variation in the relative standard deviation of the intensity of the spectral lines with the number of spectral averages in Fig. 5, the more stable data point after the turn of the curve, and the data taken too large is not conducive to practical industrial applications. So here we choose the number of spectral averages of 500 as measurements.

3.4 Quantitative analysis

3.4.1 Comparison of the effects of different background deductions. Both algorithms work by selecting a sliding window within which to process the data. The major difference between the two is that the MF algorithm performs noise reduction by de-mediating the inside of the window. The SG algorithm, on the other hand, does a polynomial least squares fit to the data within the window.

As can be seen from Fig. 6, the original LIBS spectrum has more noise signals and the spectrum is noisy; the smoothing of the spectrum after the MF correction improved significantly, retaining the main information of the original spectrum and reducing the overall intensity; SG corrected smoothing reduces the spectral noise, but not as much as MF corrected, and is almost identical to the original spectrum in terms of main information and maximum fidelity.

3.4.2 Calculation of the detection limit. The limit of detection (LOD) is an important metric for evaluating the quantitative analytical performance of the LIBS technique, and here, it is defined intuitively as the lowest concentration that can be detected by this method. The LOD of the element is based on the universal $3\sigma_B$ theorem as follows:

$$\mathrm{LOD} = \frac{3\sigma_B}{S} \tag{8}$$

where σ_B is the standard deviation of the background and S is the slope of the calibration curve.

To obtain the detection limits for different trace elements, it is necessary to obtain the slopes of the calibration curves and the standard deviations of the background signals corresponding to the different analytical lines. Here, the standard deviation of the background in a range of wavelengths where no distinct atomic lines are observed near each analytical line was approximated as the standard deviation of the background defined in the formula. The rationality of this is that there are no observable atomic or ionic lines in these two bands, and the background of the plasma is approximately continuous. Therefore, the standard deviation of the signal near the analysis line should be approximately equal to the standard deviation of the background on the analysis line. The slope of the calibration curve was obtained directly by fitting the data points in the calibration curve.

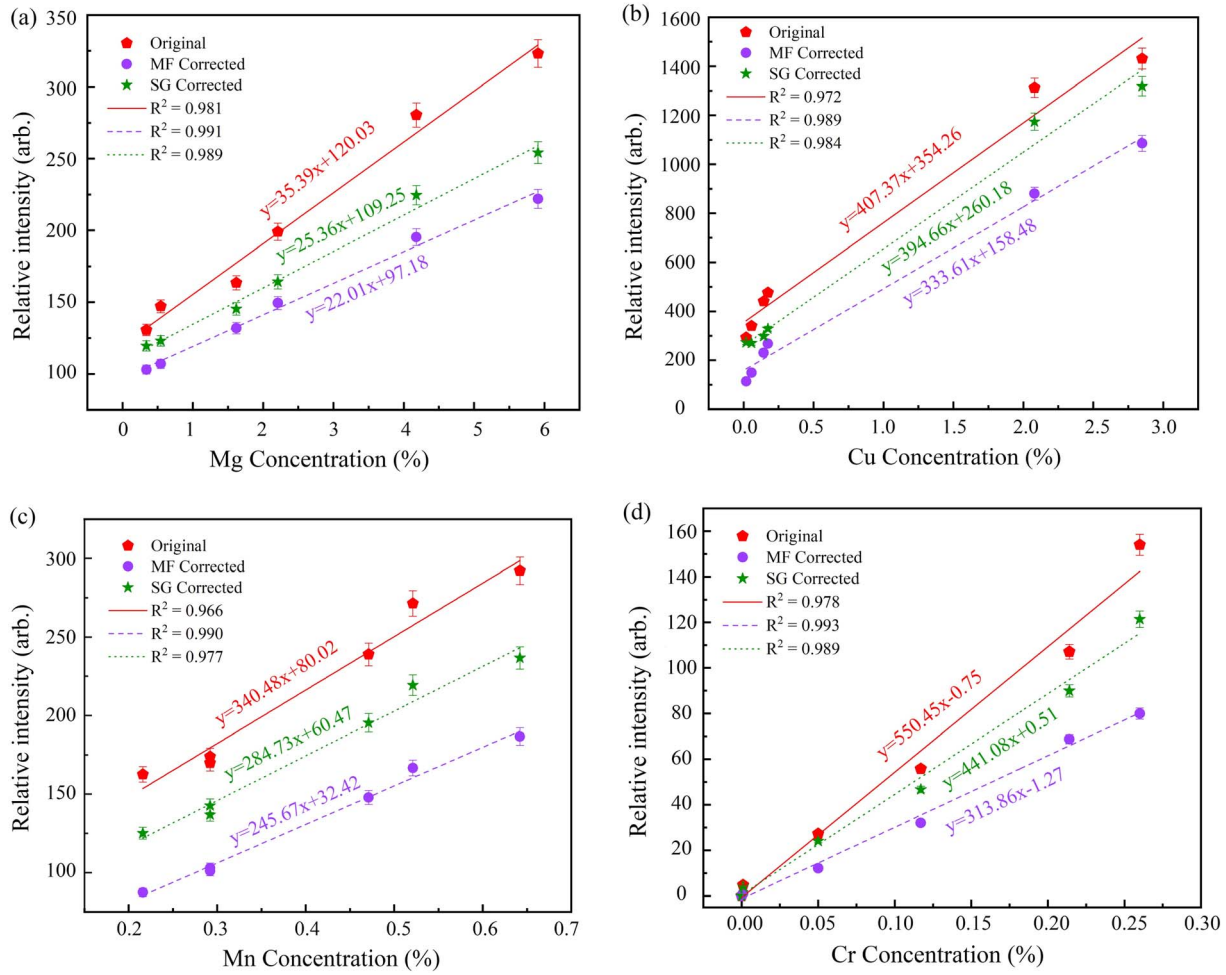

Fig. 7 Calibration curves of Mg, Cu, Mn and Cr elements in aluminum alloys obtained by MF corrected and SG corrected methods in fs-LIBS technique. (a) Mg I 285.21 nm, (b) Cu I 324.75 nm, (c) Mn I 403.44 nm, and (d) Cr I 428.97 nm.

In this set of experiments, to improve the sensitivity of trace element detection, the laser single pulse energy was chosen to be 1.5 mJ, the average number of spectral samples of the fiber optic spectrometer was 500, and the speed of the 2D platform was chosen to be 5 mm s^{-1}. The four elements Mg, Cu, Mn and Cr were quantified in aluminum alloy samples under the current experimental conditions. The analytical lines of Mg I 285.21 nm, Cu I 324.75 nm, Mn I 403.44 nm and Cr I 428.97 nm were selected for the calibration curves with the original data, MF corrected and SG corrected methods, and they are shown in Fig. 7(a)–(d), respectively. The coefficient of determination (R^2) and LOD of the calibration curve were calculated and are listed in Table 2. Table 2 and Fig. 7 show that the R^2 coefficient can reach 0.977–0.993 after background correction using both denoising algorithms. The LODs obtained with the MF correction improved by a factor of 1.4–5.2 compared to the LODs of the original data, while the LODs obtained with the SG corrected improved by a factor of 1.2–2.5 compared to the LODs of the original data.

Table 2 List of LODs of Mg, Cu, Mn and Cr elements in aluminum alloys obtained by MF corrected and SG corrected methods in fs-LIBS technique

		Σ			S			R^2			LOD (ppm)		
Element	Line (nm)	Original	MF corrected	SG corrected	Original	MF corrected	SG corrected	Original	MF corrected	SG corrected	Original	MF corrected	SG corrected
Mg	285.21	0.11	0.04	0.05	35.39	22.01	25.36	0.981	0.991	0.988	93.24	54.52	59.15
Cu	324.75	0.33	0.13	0.23	407.37	333.61	394.66	0.972	0.989	0.984	24.30	11.69	17.48
Mn	403.44	0.43	0.06	0.14	340.48	245.67	284.73	0.966	0.990	0.977	37.89	7.33	14.75
Cr	428.97	0.72	0.29	0.47	550.45	313.86	441.08	0.978	0.993	0.989	39.24	27.72	31.97

4. Conclusions

In this paper, femtosecond laser-induced breakdown spectra was used for quantitative analysis of four trace elements, Mg, Cu, Mn and Cr, in aluminum alloys. At the same time, we optimized and compared the spectral data using different filtering algorithms. The research shows that the R^2 and LOD calculated by different denoising methods are improved under fs-LIBS. The R^2 values of the linaer fit on the data after MF and SF filtering are 0.990 and 0.977, respectively. The LODs obtained using the MF algorithm and SG filtering method were 1.4–5.2 and 1.2–2.5 times better than the LODs of the original data, respectively. Therefore, the results presented in this paper showed the advantages of noise reduction of fs-LIBS data and the good prospects for signal denoising when concentrations of elements are low and features in spectra are weak. Currently, the evaluation work is being extended to a wider range of alloy materials and soil samples. Furthermore, studies on precision and more experimental variables are in progress.

Conflicts of interest

There are no conflicts to declare.

Acknowledgements

This work was financially supported by Dongguan Social Development Science and Technology Funds (20211800904632), Guangdong Basic and Applied Basic Research Foundation (2019A1515110978 & 2021B1515140018), Guangdong Province for Science and Technology Innovative Young Talents (2021KQNCX097).

Notes and references

1 R. A. Multari, D. A. Cremers, J. A. M. Dupre and J. E. Gustafson, *J. Agric. Food Chem.*, 2013, **61**, 8687–8694.
2 R. Hedwig, K. Lahna, Z. S. Lie, M. Pardede, K. H. Kurniawan, M. O. Tjia and K. Kagawa, *Appl. Opt.*, 2016, **55**, 8986–8992.
3 A. D. Giacomo, C. Koral, G. Valenza, R. Gaudiuso and M. Dell' Aglio, *J. Anal. Chem.*, 2016, **88**, 9869–9870.
4 T. B. Yuan, Z. Wang, S. L. Lui, Y. T. Fu, Z. Li, J. M. Liu and W. D. Ni, *J. Anal. At. Spectrom.*, 2013, **28**, 1045–1053.
5 S. A. Davari, S. Hu, R. Pamu and D. Mukherjee, *J. Anal. At. Spectrom.*, 2017, **32**, 1378–1387.
6 J. Rakovsky, O. Musset, J. F. Buoncristiani, V. Bichet, F. Monna, P. Neige and P. Veis, *Spectrochim. Acta, Part B*, 2012, **74–75**, 57–65.
7 J. J. Choi, S. J. Choi and J. J. Yoh, *Appl. Spectrosc.*, 2016, **70**, 1411–1419.
8 H. M. Hou, L. Cheng, T. Richardson, G. Y. Chen, M. Doeff, R. E. Zheng, R. E. Russo and V. Zorba, *J. Anal. At. Spectrom.*, 2015, **30**, 2295–2302.
9 E. C. Ferreira, J. A. G. Neto, D. M. B. P. Milori, E. J. Ferreirab and J. M. Anzanoc, *Spectrochim. Acta, Part B*, 2015, **110**, 96–99.
10 M. Wall, Z. Sun and Z. T. Alwahabi, *Opt. Express*, 2016, **24**, 1507–1517.
11 S. Tzortzakis, D. Anglos and D. Gray, *Opt. Lett.*, 2006, **31**, 1139–1141.
12 A. Botto, B. Campanella, S. Legnaioli, M. Lezzerini, G. Lorenzetti, S. Pagnotta, F. Poggialinibd and V. Palleschi, *J. Anal. At. Spectrom.*, 2019, **34**, 81–103.
13 S. Acquaviva, E. D. Anna, M. L. De Giorgi and F. Moro, *Spectrochim. Acta, Part B*, 2006, **61**, 810–816.
14 G. D. Christian, *J. Anal. Chem.*, 1969, **41**, 24A–40A.
15 G. G. A. Carvalho, J. Moros, D. Santos, F. J. Krug and J. J. Laserna, *Anal. Chim. Acta*, 2015, **876**, 26–38.
16 J. Scaffidi, W. Pearman, J. C. Carter, B. W. Colston and S. M. Angel, *Appl. Opt.*, 2004, **43**, 2786–2791.
17 L. A. Finney, P. J. Skrodzki, M. Burger, J. Nees, S. S. Harilal and I. Jovanovic, *Opt. Lett.*, 2019, **44**, 2783–2786.
18 A. K. Shaik, N. R. Epuru, H. Syed, C. Byram and V. R. Soma, *Opt. Express*, 2018, **26**, 8069–8083.
19 L. Sun and H. Yu, *Spectrochim. Acta, Part B*, 2009, **64**, 278–287.
20 D. Body and B. L. Chadwick, *Spectrochim. Acta, Part B*, 2001, **56**, 725–736.
21 J. Schlenke, L. Hildebrand, J. Moros and J. J. Laserna, *Anal. Chim. Acta*, 2012, **754**, 8–19.
22 H. Yang, L. Huang, T. B. Chen, G. F. Rao, M. H. Liu, J. Y. Chen and M. Y. Yao, *Chin. J. Anal. Chem.*, 2017, **45**, 1123–1128.
23 W. Yang, B. Li, J. Zhou, Y. Han and Q. Wang, *Appl. Opt.*, 2018, **57**, 7526–7532.
24 B. Zhang, H. Yu, L. Sun, Y. Xin and Z. Cong, *J. Appl. Spectrosc.*, 2013, **67**, 1087–1097.
25 B. Zhang, L. Sun, H. Yu, Y. Xin and Z. Cong, *Spectrochim. Acta, Part B*, 2015, **107**, 32–44.
26 K. R. Coombes, S. Tsavachidis, J. S. Morris, K. A. Baggerly, M. C. Hung and H. M. Kuerer, *Proteomics*, 2005, **5**, 4107–4117.
27 H. G. Schulze, R. B. Foist, A. Ivanov and R. F. B. Turner, *J. Appl. Spectrosc.*, 2008, **62**, 1160–1166.
28 J. Kang, R. H. Li, Y. R. Wang, Y. Q. Chen and Y. X. Yang, *J. Anal. At. Spectrom.*, 2017, **32**, 2292.